

# Probing the resonance in the Dirac equation with quadruple-deformed potentials by complex momentum representation method

Zhi Fang,<sup>1</sup> Min Shi,<sup>1,2</sup> Jian-You Guo,<sup>1,\*</sup> Zhong-Ming Niu,<sup>1,3</sup> Haozhao Liang,<sup>2,3,4</sup> and Shi-Sheng Zhang<sup>5</sup>

<sup>1</sup>*School of Physics and Materials Science, Anhui University, Hefei 230601, P.R.China*

<sup>2</sup>*RIKEN Nishina Center, Wako 351-0198, Japan*

<sup>3</sup>*Interdisciplinary Theoretical Science Research Group, RIKEN, Wako 351-0198, Japan*

<sup>4</sup>*Department of Physics, Graduate School of Science,  
The University of Tokyo, Tokyo 113-0033, Japan*

<sup>5</sup>*School of Physics and Nuclear Energy Engineering, Beihang University, Beijing 100191, China*

(Dated: August 10, 2018)

Resonance plays critical roles in the formation of many physical phenomena, and many techniques have been developed for the exploration of resonance. In a recent letter [Phys. Rev. Lett. 117, 062502 (2016)], we proposed a new method for probing single-particle resonances by solving the Dirac equation in complex momentum representation for spherical nuclei. Here, we extend this method to deformed nuclei with theoretical formalism presented. We elaborate numerical details, and calculate the bound and resonant states in <sup>37</sup>Mg. The results are compared with those from the coordinate representation calculations with a satisfactory agreement. In particular, the present method can expose clearly the resonant states in complex momentum plane and determine precisely the resonance parameters for not only narrow resonances but also broad resonances that were difficult to obtain before.

PACS numbers: 21.60.Jz, 21.10.Pc, 25.70.Ef

## I. INTRODUCTION

Resonance is one of the most striking phenomena in the whole range of scattering experiments and appears widely in atomic, molecular, and nuclear physics [1]. Resonance plays critical roles in the formation of many physical phenomena such as the quantum halos [2]. Theoretical explanation of halo in <sup>11</sup>Li [3], prediction of giant halo in Zr and Ca isotopes [4, 5], and understanding of deformed halo in <sup>31</sup>Ne and <sup>44</sup>Mg [6, 7] are mainly attributed to consider the contributions from the continuum, especially the resonances in the continuum. The change of traditional magic numbers in these nuclei with unusual neutron-to-proton ratio can be understood in terms of the shell structure of resonant levels [8]. It is also found that the contribution of the continuum to the giant resonances mainly comes from single-particle resonances [9, 10]. Resonance is also closely relevant to the nucleosynthesis of chemical elements in the Universe [11, 12]. Therefore, research on resonance is one of the hottest topics in different branches of physics.

So far, a series of methods have been proposed for resonance, including the scattering phase shift method, the analytic continuation in the coupling constant (ACCC) approach, *R*-matrix method, *S*-matrix method, Green's function method, etc. These methods have gained success in handling unbound problems. Even so, one hopes to establish a unified theory, which can deal with both bound states and resonant states on the same footing. The complex scaled method (CSM) introduced in Refs. [13] would satisfy this requirement.

In the CSM, the wave functions adopted for the resonant states are square-integrable, and thus it is not necessary to use the asymptotic boundary conditions. Moreover, the complex scaled equation can be solved by using the bound-state methods, in which the bound states and resonant states are processed equally. These advantages enable the application of CSM to different theoretical frameworks, including the combinations with the few-body models [14], shell models [15, 16], and Hartree-Fock theories [17, 18]. More applications can be found in Refs. [19–21]. Recently, we have applied the CSM to explore the resonances in spherical nuclei [22–25] and deformed nuclei [26–28] in a satisfactory agreement with those obtained by other methods.

Although it can describe the bound states and resonant states in a unified way, the CSM still has some shortcomings. For example, in order to determine accurately the resonance parameters, repeated diagonalization of the Hamiltonian is required in the complex scaling calculations. In addition, the CSM is only applicable to the dilation analytic potentials. For the systems like nuclei, the mean-field potentials for nucleon movement are similar to the Woods-Saxon potentials. There appear singularities when the complex rotation angle  $\theta = \tan^{-1}(\pi a/R)$ . Hence, the CSM

---

\*E-mail: jianyong@ahu.edu.cn

is only effective in the interval of  $0 < \theta < \tan^{-1}(\pi a/R)$  for the resonances in nuclei, which confines the application of the CSM for very broad resonances, while the broad resonances deserve more attentions for their roles in exotic phenomena.

In order to hold the advantages of CSM and avoid its shortcomings, the complex momentum representation (CMR) method has been proposed. In Ref. [29], the Schrödinger equation was formalized using momentum representation. This method has avoided all the defects in the CSM, and has been used to explore the bound states [30, 31] and resonant states [32, 33] in the nonrelativistic case, and used as the so-called ‘‘Berggren representation’’ in the shell-model calculations [34, 35]. Considering that the relativistic resonances are widely concerned, almost all the methods for resonances have been extended to the relativistic framework [36–42], including the relativistic CSM [22, 27] and relativistic complex scaled Green’s function method [25]. Recently, we applied the CMR method to the relativistic mean-field (RMF) framework and established the RMF-CMR method for the resonances in the spherical case [43], in which both bound states and resonant states have been treated on the same footing. The RMF-CMR method gathers the advantages of the RMF and CMR, and is able to describe self-consistently nuclear bound states and resonant states in the relativistic framework. Due to these advantages, to extend the method to deformed nuclei is worthwhile as most of nuclei with deformation.

In this paper we develop the relativistic version of CMR method for deformed nuclei, in which the Dirac equation describing deformed nuclei is processed into a set of coupled differential equations by the coupled-channel method and the set of coupled differential equations are solved using the complex momentum representation technique. We will first present the theoretical formalism, and then elaborate numerical details. Taking the nucleus  $^{37}\text{Mg}$  as an example, we calculate the bound and resonant states, and compare with those obtained in coordinate representation with the ACCC method.

## II. FORMALISM

Considering that the relativistic mean-field theory is very successful in describing various nuclear phenomena [44–50] and nuclear inputs in astrophysics [51–55], we explore the single-particle resonances in deformed nuclei based on the relativistic mean-field theory with the Dirac equation as

$$[\vec{\alpha} \cdot \vec{p} + \beta (M + S) + V] \psi = \varepsilon \psi, \quad (1)$$

where  $M$  ( $\vec{p}$ ) is the nucleon mass (momentum),  $\vec{\alpha}$  and  $\beta$  are the Dirac matrices, and  $S$  and  $V$  are the scalar and vector potentials, respectively. The details of the RMF theory can refer to the literatures [44–47].

The solutions of Eq. (1) include the bound states, resonant states, and nonresonant continuum. The bound states can be obtained with conventional methods. For the resonant states, many techniques have been developed, while some of them exist certain shortcomings. In Ref. [43], we proposed a new method by solving the Dirac equation in complex momentum representation for spherical nuclei. In the present work, we extend this method to deformed nuclei. Without loss of generality, only the axially symmetrical quadruple deformation is considered here,  $V(\vec{r})$  and  $S(\vec{r})$  are taken as

$$\begin{cases} V(\vec{r}) = V_0 f(r) - \beta_2 V_0 k(r) Y_{20}(\vartheta, \varphi), \\ S(\vec{r}) = S_0 f(r) - \beta_2 S_0 k(r) Y_{20}(\vartheta, \varphi), \end{cases} \quad (2)$$

where  $\beta_2$  is the quadruple deformation parameter. Similar to Ref. [56], a Woods-Saxon type potential is adopted with  $f(r) = \frac{1}{1 + \exp[(r-R)/a]}$  and  $k(r) = \frac{r df(r)}{dr}$ . In order to explore the resonances in deformed nuclei, we transform Eq. (1) into momentum representation as

$$\int d\vec{k}' \langle \vec{k} | H | \vec{k}' \rangle \psi(\vec{k}') = \varepsilon \psi(\vec{k}), \quad (3)$$

where  $H = \vec{\alpha} \cdot \vec{p} + \beta (M + S) + V$  is the Dirac Hamiltonian,  $\psi(\vec{k})$  is the corresponding wave function in momentum representation, and  $|\vec{k}\rangle$  represents the wave function of a free particle with wave vector  $\vec{k} = \vec{p}/\hbar$ . In order to solve the Dirac equation (3) for deformed system, the coupled-channel method is adopted, the wave function is expanded as

$$\psi(\vec{k}) = \psi_{m_j}(\vec{k}) = \sum_{lj} \begin{pmatrix} f^{lj}(k) \phi_{ljm_j}(\Omega_k) \\ g^{lj}(k) \phi_{ljm_j}(\Omega_k) \end{pmatrix}, \quad (\tilde{l} = 2j - l) \quad (4)$$

with

$$\phi_{ljm_j}(\Omega_k) = \sum_{m_s} \langle lm \frac{1}{2} m_s | jm_j \rangle Y_{lm}(\Omega_k) \chi_{m_s},$$

where  $f^{lj}(k)$  and  $g^{lj}(k)$  are the radial components of Dirac spinors in momentum representation,  $l$  and  $m$  are the quantum numbers of the orbital angular momentum and its projection on the third axis,  $j$  and  $m_j$  are the quantum numbers of the total angular momentum and its projection on the third axis, and  $\chi_{m_s}$  is the spin wave function with the third component of spin angular momentum  $m_s$ . It should be emphasized that the projection of the total angular momentum on the third axis  $m_j$  and the parity  $\pi$  are good quantum numbers for an axially deformed system.

Putting the wave function (4) into the equation (3), the Dirac equation becomes

$$\begin{cases} M f^{lj}(k) - k g^{lj}(k) + \sum_{l'j'} \int k'^2 dk' V^+(l', j', p, q, l, j, m_j, k, k') f^{l'j'}(k') = \varepsilon f^{lj}(k), \\ -k f^{lj}(k) - M g^{lj}(k) + \sum_{l'j'} \int k'^2 dk' V^-(\tilde{l}', j', p, q, \tilde{l}, j, m_j, k, k') g^{l'j'}(k') = \varepsilon g^{lj}(k), \end{cases} \quad (5)$$

with

$$\begin{aligned} & V^+(l', j', p, q, l, j, m_j, k, k') \\ &= (-)^l i^{l+l'} \frac{2}{\pi} \int r^2 dr [V(r) + S(r)] j_l(kr) j_{l'}(k'r) \sum_{m_s} \langle lm | Y_{pq}(\Omega_r) | l'm' \rangle \langle lm \frac{1}{2} m_s | jm_j \rangle \langle l'm' \frac{1}{2} m_s | j'm_j \rangle, \end{aligned} \quad (6)$$

$$\begin{aligned} & V^-(\tilde{l}', j', p, q, \tilde{l}, j, m_j, k, k') \\ &= (-)^{\tilde{l}} i^{\tilde{l}+\tilde{l}'} \frac{2}{\pi} \int r^2 dr [V(r) - S(r)] j_{\tilde{l}}(kr) j_{\tilde{l}'}(k'r) \sum_{m_s} \langle \tilde{l}\tilde{m} | Y_{pq}(\Omega_r) | \tilde{l}'\tilde{m}' \rangle \langle \tilde{l}\tilde{m} \frac{1}{2} m_s | jm_j \rangle \langle \tilde{l}'\tilde{m}' \frac{1}{2} m_s | j'm_j \rangle, \end{aligned} \quad (7)$$

where  $j_l(kr)$  [ $j_{\tilde{l}}(kr)$ ] are the spherical Bessel functions of order  $l$  [ $\tilde{l}$ ]. Equation (5) is a set of coupled integral equations. Its solution is difficult to obtain by the conventional methods especially for the resonant states. By turning the momentum integral into a sum over a finite set of points  $k$  and  $dk$  with a set of weights  $w$ , the integral equation (5) becomes a matrix equation

$$\begin{cases} M f^{lj}(k_a) - k_a g^{lj}(k_a) + \sum_{l'j'} \sum_b w_b k_b^2 V^+(l', j', p, q, l, j, m_j, k_a, k_b) f^{l'j'}(k_b) = \varepsilon f^{lj}(k_a), \\ -k_a f^{lj}(k_a) - M g^{lj}(k_a) + \sum_{l'j'} \sum_b w_b k_b^2 V^-(\tilde{l}', j', p, q, \tilde{l}, j, m_j, k_a, k_b) g^{l'j'}(k_b) = \varepsilon g^{lj}(k_a). \end{cases} \quad (8)$$

In Eq. (8), the Hamiltonian matrix is not symmetric. For simplicity in computation, we symmetrize it by the following transformation

$$\begin{cases} \mathbf{f}(k_a) = \sqrt{w_a} k_a f(k_a), \\ \mathbf{g}(k_a) = \sqrt{w_a} k_a g(k_a), \end{cases} \quad (9)$$

which gives us a symmetric matrix in the momentum representation as

$$\begin{cases} \sum_b \left[ M \delta_{ab} \mathbf{f}^{lj}(k_b) + \sum_{l'j'} \sqrt{w_a w_b} k_a k_b V^+(l', j', p, q, l, j, m_j, k_a, k_b) \mathbf{f}^{l'j'}(k_b) - k_a \delta_{ab} \mathbf{g}^{lj}(k_b) \right] = \varepsilon \mathbf{f}^{lj}(k_a), \\ \sum_b \left[ -k_a \delta_{ab} \mathbf{f}^{lj}(k_b) - M \delta_{ab} \mathbf{g}^{lj}(k_b) + \sum_{l'j'} \sqrt{w_a w_b} k_a k_b V^-(\tilde{l}', j', p, q, \tilde{l}, j, m_j, k_a, k_b) \mathbf{g}^{l'j'}(k_b) \right] = \varepsilon \mathbf{g}^{lj}(k_a). \end{cases} \quad (10)$$

So far, to solve the Dirac equation (1) becomes an eigensolution problem of the symmetric matrix. All the bound and resonant states can be obtained simultaneously by diagonalizing the Hamiltonian in Eq. (10). Compared with Refs. [56, 57], where the bound solutions are obtained by solving a set of coupled differential equations and every resonant state is handled solely by the scattering phase shift method or ACCC approach, there is no doubt that the present method is more convenient.

The diagonalization of the Hamiltonian matrix in Eq. (10) can provide us the energies and wave functions in the momentum representation. If we regard the wave functions in the coordinate representation, the following transformation is introduced

$$\psi(\vec{r}) = \langle \vec{r} | \psi \rangle = \frac{1}{(2\pi)^{3/2}} \int d\vec{k} e^{i\vec{k}\cdot\vec{r}} \psi(\vec{k}). \quad (11)$$

For an axially deformed nucleus, putting the wavefunctions (4) into the equation (11), we obtain the Dirac spinors in the coordinate space as

$$\psi(\vec{r}) = \psi_{m_j}(\vec{r}) = \sum_{lj} \begin{pmatrix} f^{lj}(r)\phi_{ljm_j}(\Omega_r) \\ g^{lj}(r)\phi_{\bar{l}jm_j}(\Omega_r) \end{pmatrix}, \quad (12)$$

with the radial components

$$\begin{cases} f^{lj}(r) = i^l \sqrt{\frac{2}{\pi}} \sum_a \sqrt{w_a} k_a j_l(k_a r) \mathbf{f}^{lj}(k_a), \\ g^{lj}(r) = i^{\bar{l}} \sqrt{\frac{2}{\pi}} \sum_a \sqrt{w_a} k_a j_{\bar{l}}(k_a r) \mathbf{g}^{lj}(k_a). \end{cases}$$

### III. NUMERICAL DETAILS AND RESULTS

Based on the preceding formalism, we explore the resonances in real nuclei. Before starting these calculations, we clarify several key points: (i) the coupled-channel method is adopted in solving the Dirac equation for deformed nuclei, where the wave functions are expanded with different channels labelled as  $lj$ . The sum over  $lj$  in Eq. (4) needs to be restricted to a limited number  $N_c$ ; (ii) the momentum integral in Eq. (5) is from zero to infinity, it needs to be truncated into a large enough momentum  $k_{\max}$ . When  $k_{\max}$  is fixed, the integral can be calculated by a sum shown in Eq. (10). As a sum with evenly spaced  $dk$  and a constant weight  $w_a$  converges slowly, here it is replaced by the Gauss-Legendre quadrature with a finite grid number  $N_l$ . Through these processions, the Hamiltonian in Eq. (10) becomes a  $2N_c N_l \times 2N_c N_l$  matrix. In the actual calculations, the momentum is truncated to  $k_{\max} = 4.0 \text{ fm}^{-1}$ , which is sufficient for all the concerned resonances. The grid number of the Gauss-Legendre quadrature  $N_l = 120$  is used for the momentum integral along the contour, which is enough to ensure the convergence with respect to numbers of discretization points. The coupled-channel number  $N_c = 8$  is taken for the wave function expansions, which is enough to ensure the required precision.

With these parameters designed, we explore the resonances in deformed nuclei with  $^{37}\text{Mg}$  as an example. For the comparison with the ACCC calculations, the parameters in the scalar potential  $S$  and vector potential  $V$  adopted are the same as those in Ref. [57]. The Dirac equation is solved by diagonalizing the  $2N_c N_l \times 2N_c N_l$  matrix in Eq. (10) along an appropriate contour of momentum integral. The contour is required to be large enough to expose all the concerned resonances.

To single out a large enough contour, we first check the dependence of the calculations on the contour. For this purpose, we have explored the resonant states in  $^{37}\text{Mg}$  with four different contours, which are displayed in Fig. 1 for the states  $\Omega^\pi = 1/2^-$  with  $\beta_2 = 0.4$ . Similar to the spherical case [43], the resonant states have nothing to do with the choice of the contour. With the change of integral contour, the continuous spectra follow the contour, while the resonant states always stay at their original positions. When the contour becomes deeper from the magenta color to the blue color, the continuous spectra drop down with the contour, the resonant state  $1/2[301]$  does not move. Similarly, when the contour moves from left (red color) to right (olive color) or from right to left, the continuous spectra follow the contour, while the resonant states  $1/2[301]$  and  $1/2[321]$  remain their own positions. These indicate that the physical resonant states obtained by the present method are indeed independent on the contour. Hence, we can select a large enough contour to expose all the concerned resonances. This conclusion is in agreement with that in the spherical case [43].

Using the triangle contour with the four points  $k = 0 \text{ fm}^{-1}$ ,  $k = 0.5 - i0.5 \text{ fm}^{-1}$ ,  $k = 1.0 \text{ fm}^{-1}$ , and  $k_{\max} = 4.0 \text{ fm}^{-1}$ , all the concerned bound and resonant states in  $^{37}\text{Mg}$  can be obtained over the range of deformation. An illustrated result is displayed in Fig. 2 for the states  $\Omega^\pi = \frac{1}{2}^\pm, \frac{3}{2}^\pm, \dots, \frac{9}{2}^\pm$  with  $\beta_2 = -0.2$ . From Fig. 2, it can be seen that the bound states are exposed clearly on the imaginary axis, the resonant states are isolated from the continuum in the fourth quadrant, and the continuous spectra follow the integral contour. In the region of resonant states, there are fifteen resonant states exposed in the present calculations. Some resonant states are close to the real  $k$  axis, which correspond to the narrow resonances with smaller width. Some other resonant states are far away from the real  $k$  axis, which are broad resonances. In other words, the current calculations have provided us not only the narrow resonances but also the broad resonances as long as the momentum contour covers the range of resonances.

As we focus on the resonances in the deformed nuclei, it is interesting to observe intuitively the dependence of resonances on deformation. In Fig. 3, we show the  $\Omega^\pi = \frac{1}{2}^\pm, \frac{3}{2}^\pm, \dots, \frac{9}{2}^\pm$  resonant states with several different deformations. When  $\beta_2 = 0$ , the system is spherically symmetric, there appear four resonant states  $2p_{1/2}$ ,  $2d_{5/2}$ ,  $1f_{5/2}$ , and  $1g_{9/2}$  in the complex momentum plane. When the spherical symmetry is broken, the degenerate states  $2d_{5/2}$  and  $1f_{5/2}$  respectively split into three resonant states and the degenerate state  $1g_{9/2}$  into five resonant states.

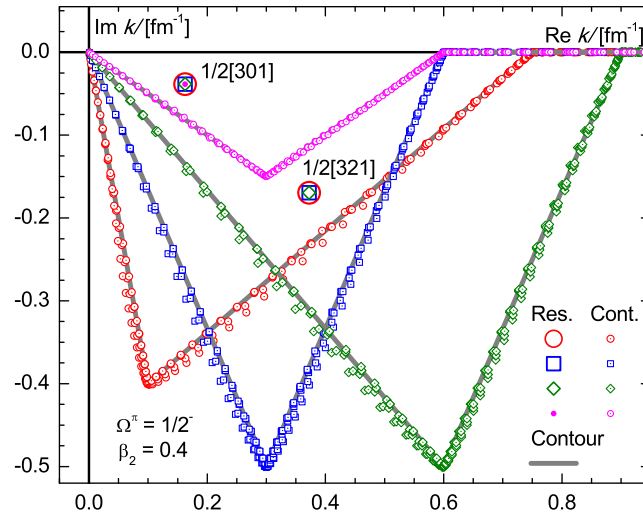


FIG. 1: (Color online) Single-particle spectra in  $^{37}\text{Mg}$  for the states  $\Omega^\pi = 1/2^-$  with  $\beta_2 = 0.4$  in the complex  $k$  plane with four different contours. The open red circles, blue squares, olive diamonds, and magenta dots represent the resonances obtained in four different contours, respectively. The smaller labels with a dot inside represent the continuum. The gray lines represent the corresponding contours of momentum integral.

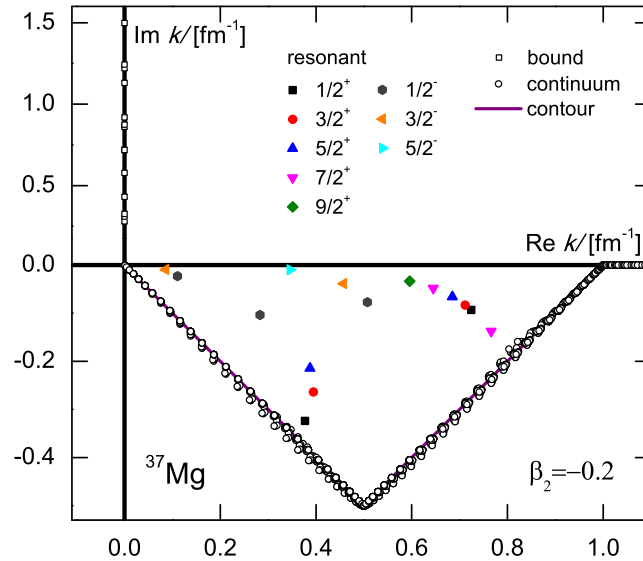


FIG. 2: (Color online) Single-particle spectra in  $^{37}\text{Mg}$  for the states  $\Omega^\pi = \frac{1}{2}^\pm, \frac{3}{2}^\pm, \dots, \frac{9}{2}^\pm$  with  $\beta_2 = -0.2$  in the complex momentum plane. The bound states, resonant states with different quantum numbers, and continuum are marked with different labels, while the purple solid line represents the contour of momentum integral in complex momentum plane.

Their positions in the complex momentum plane depend on the deformation. With the development of deformation, some resonant states disappear and some other resonant states appear in the current region of momentum, which can be found in Fig. 3 with  $\beta_2 = 0.2$ .

From Figs. 2 and 3, it is seen that the bound states and resonant states together with their evolutions to deformation can be obtained in the present calculations. For the resonant states, we can read the real and imaginary parts of their wavevectors from the complex  $k$  plane, and then we can calculate the resonance parameters like energy and width in terms of  $E_r + iE_i = E_r - i\Gamma/2 = \sqrt{k^2 + M^2} - M$ . The calculated single-particle energies varying with deformation is shown in Fig. 4 for the bound states and resonant states, where the bound levels are marked by the solid line and the resonant levels by the dashed lines with the Nilsson labels on the lines and the corresponding spherical labels in the position  $\beta_2 = 0$ . For the resonant states, we show the single-particle energies in Fig. 4 together with the corresponding widths in Fig. 5.

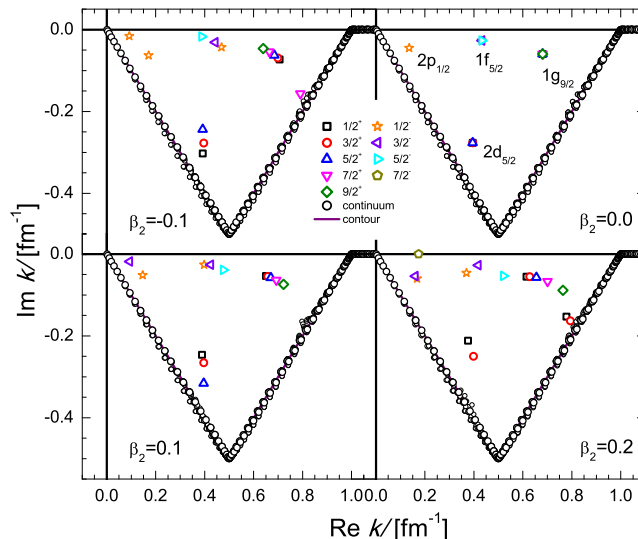


FIG. 3: (Color online) Single-particle resonances for the states  $\Omega^\pi = \frac{1}{2}^\pm, \frac{3}{2}^\pm, \dots, \frac{9}{2}^\pm$  in the complex momentum plane with several different deformations. The outstanding labels denote the resonant states with the corresponding quantum numbers, while the black open circles and purple solid line represent the continuum and the integral contour in the complex momentum plane, respectively.

In comparison with the coupled-channel calculations in the coordinate representation, on one hand, it is found that all the available bound levels and their evolutions to  $\beta_2$  are the fully same as those shown in Ref. [57]. For the resonant levels, our results are also in agreement with those obtained by the ACCC in Ref. [57]. On the other hand, in addition to the levels with the spherical labels  $1f_{7/2}$ ,  $2p_{3/2}$ ,  $2p_{1/2}$ , and  $1f_{5/2}$ , we also have obtained the resonant levels with the spherical labels  $2d_{5/2}$  and  $1g_{9/2}$ . Especially for the states with the spherical label  $2d_{5/2}$  which locate at the middle of  $2p_{1/2}$  and  $1f_{5/2}$ , the calculations in Ref. [57] have not given out the results on these states. Furthermore, a notable phenomenon appears in the resonant level  $5/2[402]$ . With the increasing of deformation in the prolate side, its energy drops down while its width goes up rapidly. Eventually, the resonant state disappears at the large deformation, since it is difficult for particle to populate on the level with too short life time.

The evolution of the widths to deformation for the concerned resonant states is shown in Fig. 5. Similar to the energies, there exists the shell structure in these widths. Especially for the spherical case, the gap appearing in the widths between  $2d_{5/2}$  and  $1g_{9/2}$  is very large. Compared with the energy, the order is different for the width. Namely, although the energies of the  $2d_{5/2}$  states are lower, the corresponding widths are larger due to the smaller centrifugal barrier.

In addition to the energy spectra, we have also obtained the wave functions for deformed nuclei in the momentum space. In Fig. 6, we show the radial-momentum probability distributions (RMPD) for the single-particle states  $\Omega^\pi = 5/2^+$  with the quadruple deformation  $\beta_2 = 0.3$ . It can be seen that there are two single-particle states with their RMPD expanded much wider than the surrounding states. By checking their energies, it is found that the blue dashed line corresponds to the bound state  $5/2[202]$  and the red solid line is the resonant state  $5/2[422]$ . The other states, their RMPD display sharp peaks at different values of  $k$ , corresponding to the free particles. These results agree with the Heisenberg uncertainty principle: a less well-defined momentum corresponds to a more well-defined position for the bound and resonant states; and a well-defined momentum corresponds to a less well-defined position for the free particles. In the actual calculations, we have obtained many single-particle states corresponding to the free particles. Note that to make the RMPD clear, only a part of free states are displayed in the figure.

With these wave functions in the momentum space obtained, we can transform them into the coordinate space by using Eq. (12). In Fig. 7, we have shown the radial density distributions in the coordinate space for the bound states  $1/2[110]$  and  $1/2[310]$ , and the resonant state  $1/2[301]$  with  $\beta_2 = 0.4$ , where the four contours are the same as those in Fig. 1. Whether bound states or resonant states, the radial density distributions in the coordinate space are independent of the contour, while those of continuous spectra depend on the contour.

The above results indicate that the present method is applicable and efficient for exploring the resonances in both spherical and deformed nuclei. Comparing with those frequently used methods that are only effective for the narrow resonances, the present method is superior because it is not only appropriate for the narrow resonance, but also can be reliably applied to the broad resonances that were difficult to obtain before.

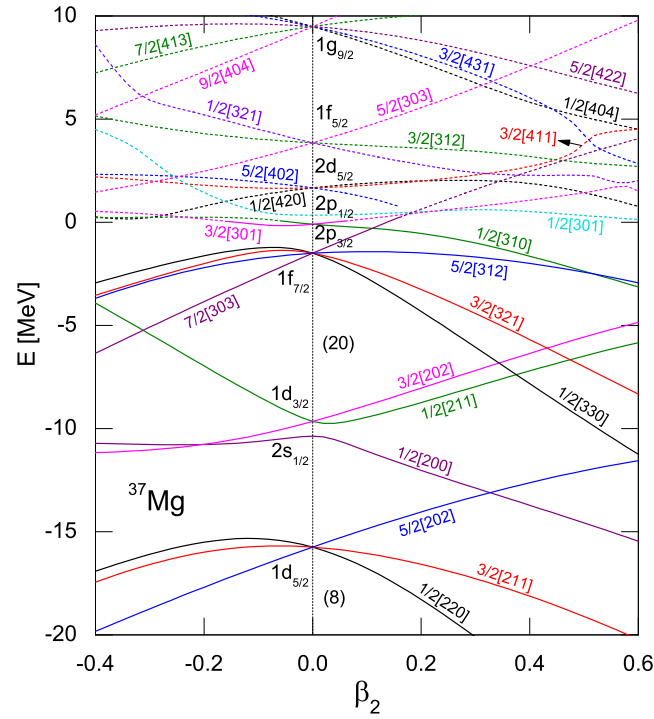


FIG. 4: (Color online) The evolution of single-particle energies to deformation for all the concerned bound and resonant states, where the bound states are marked by the solid lines and the resonant states by the dashed lined with the Nilsson labels on the lines and the corresponding spherical labels in the position  $\beta_2 = 0$ .

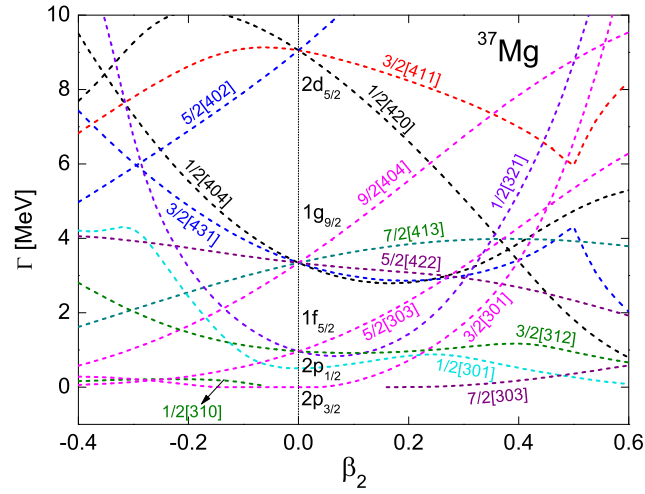


FIG. 5: (Color online) The evolution of widths to deformation for all the concerned resonant states. They are marked by the color dashed lines with the Nilsson labels on the lines and the corresponding spherical labels in the position  $\beta_2 = 0$ .

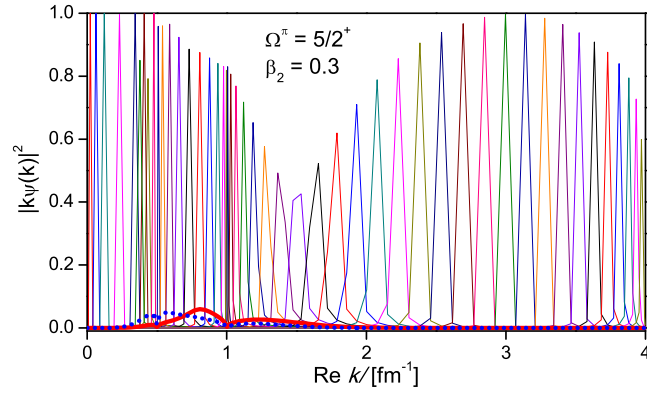


FIG. 6: (Color online) Radial-momentum probability distributions for the states  $\Omega^\pi = 5/2^+$  with  $\beta_2 = 0.3$ , where the blue dashed line and red solid line correspond respectively to the bound state and resonant state, and the others correspond to the background of the continuum.

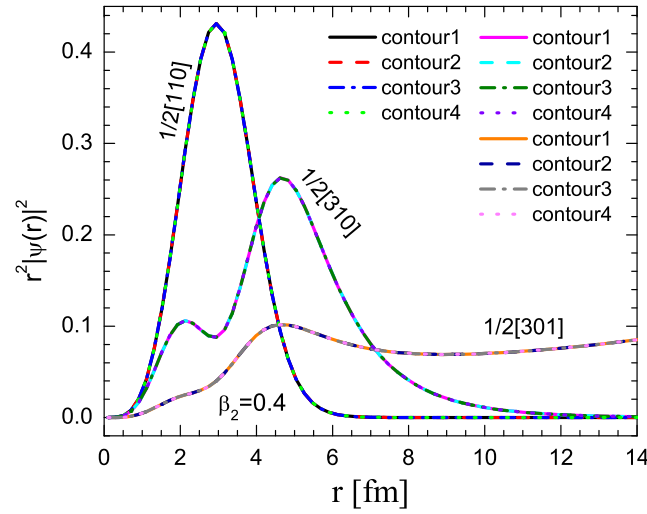


FIG. 7: (Color online) Radial density distributions in the coordinate space for the bound states  $1/2[110]$  and  $1/2[310]$ , and the resonant state  $1/2[301]$  with  $\beta_2 = 0.4$ , where the four contours are the same as those in Fig. 1.



#### IV. SUMMARY

In summary, we have developed a new method to explore the resonances for deformed nuclei by solving the Dirac equation in complex momentum representation. In this scheme, the Dirac equation describing deformed nuclei is processed into a set of coupled differential equations by the coupled-channel method. The set of coupled differential equations is then solved by using the complex momentum representation technique, which makes the solutions of Dirac equation become the diagonalization of a matrix. This method describes the bound states and resonant states on the equal footing, which greatly simplifies the problem of how to handle the unbound states for deformed systems.

We have presented the theoretical formalism, elaborated the numerical details, and discussed the dependence of the calculations on the contour of momentum integral, and the satisfactory results are obtained in comparison with the coordinate representation calculations. As an illustrated example, we have explored the resonances in  $^{37}\text{Mg}$  and obtained the energies and widths of single-particle resonant states and their evolutions to the deformation. Compared with the CSM and ACCC calculations, the agreeable results are obtained for narrow resonances. However, for broad resonances that are difficult to be obtained by other methods, the present method is also applicable and effective.

#### V. ACKNOWLEDGMENTS

This work was partly supported by the National Natural Science Foundation of China under Grant Nos. 11575002, 11175001, 11205004, 11305002, and 11375022; the Program for New Century Excellent Talents at the University of China under Grant No. NCET-05-0558; the Natural Science Foundation of Anhui Province under Grant No. 1408085QA21; the Key Research Foundation of Education Ministry of Anhui Province of China under Grant No. KJ2016A026; and the 211 Project of Anhui University.

- 
- [1] J. R. Taylor, *Scattering Theory: The Quantum Theory on Nonrelativistic Collisions* (John Wiley & Sons, New York, 1972).
  - [2] A. S. Jensen, K. Riisager, D. V. Fedorov, and E. Garrido, *Rev. Mod. Phys.* **76**, 215 (2004).
  - [3] J. Meng and P. Ring, *Phys. Rev. Lett.* **77**, 3963 (1996).
  - [4] J. Meng and P. Ring, *Phys. Rev. Lett.* **80**, 460 (1998).
  - [5] J. Meng, H. Toki, J. Y. Zeng, S. Q. Zhang, and S.-G. Zhou, *Phys. Rev. C* **65**, 041302(R) (2002).
  - [6] I. Hamamoto, *Phys. Rev. C* **81**, 021304 (2010).
  - [7] S. G. Zhou, J. Meng, P. Ring, and E. G. Zhao, *Phys. Rev. C* **82**, 011301 (2010).
  - [8] I. Hamamoto, *Phys. Rev. C* **85**, 064329 (2012).
  - [9] P. Curutchet, T. Vertse, and R. J. Liotta, *Phys. Rev. C* **39**, 1020 (1989).
  - [10] L. G. Cao and Z. Y. Ma, *Phys. Rev. C* **66**, 024311 (2002).
  - [11] S. S. Zhang, M. S. Smith, G. Arbanas, and R. L. Kozub, *Phys. Rev. C* **86**, 032802(R) (2012).
  - [12] T. Faestermann, P. Mohr, R. Hertenberger, and H.-F. Wirth, *Phys. Rev. C* **92**, 052802(R) (2015).
  - [13] J. Aguilar and J. M. Combes, *Commun. Math. Phys.* **22**, 269 (1971); E. Balslev and J. M. Combes, *Commun. Math. Phys.* **22**, 280 (1971); B. Simon, *Commun. Math. Phys.* **27**, 1 (1972).
  - [14] K. Arai, *Phys. Rev. C* **74**, 064311 (2006).
  - [15] N. Michel, K. Matsuyanagi, and M. Stoitsov, *Phys. Rev. C* **78**, 044319 (2008).
  - [16] N. Michel, W. Nazarewicz, M. Ploszajczak, and T. Vertse, *J. Phys. G* **36**, 013101 (2009).
  - [17] A. T. Kruppa, P. H. Heenen, H. Flocard, and R. J. Liotta, *Phys. Rev. Lett.* **79**, 2217 (1997).
  - [18] A. T. Kruppa, G. Papadimitriou, W. Nazarewicz, and N. Michel, *Phys. Rev. C* **89**, 014330 (2014).
  - [19] N. Moiseyev, *Phys. Rep.* **302**, 212 (1998).
  - [20] T. Myo, Y. Kikuchi, H. Masui, and K. Katō, *Prog. Part. Nucl. Phys.* **79**, 1 (2014).
  - [21] J. Carbonell, A. Deltuva, A. C. Fonseca, and R. Lazauskas, *Prog. Part. Nucl. Phys.* **74**, 55 (2014).
  - [22] J. Y. Guo, X. Z. Fang, P. Jiao, J. Wang, and B. M. Yao, *Phys. Rev. C* **82**, 034318 (2010).
  - [23] J. Y. Guo, M. Yu, J. Wang, B. M. Yao, and P. Jiao, *Comput. Phys. Commun.* **181**, 550 (2010).
  - [24] Z. L. Zhu, Z. M. Niu, D. P. Li, Q. Liu, and J. Y. Guo, *Phys. Rev. C* **89**, 034307 (2014).
  - [25] M. Shi, J. Y. Guo, Q. Liu, Z. M. Niu, and T. H. Heng, *Phys. Rev. C* **92**, 054313 (2015).
  - [26] Q. Liu, J. Y. Guo, Z. M. Niu, and S. W. Chen, *Phys. Rev. C* **86**, 054312 (2012).
  - [27] M. Shi, Q. Liu, Z. M. Niu, and J. Y. Guo, *Phys. Rev. C* **90**, 034319 (2014).
  - [28] X. X. Shi, M. Shi, Z. M. Niu, T. H. Heng, and J. Y. Guo, *Phys. Rev. C* **94**, 024302 (2016).
  - [29] T. Berggren, *Nucl. Phys. A* **109**, 265 (1968).
  - [30] C. V. Sukumar, *J. Phys. A* **12**, 1715 (1979).
  - [31] Y. R. Kwon and F. Tabakin, *Phys. Rev.* **18**, 932 (1978).
  - [32] G. Hagen and J. S. Vaagen, *Phys. Rev. C* **73**, 034321 (2006).
  - [33] A. Deltuva, *Few-Body Syst.* **56**, 897 (2015).

- [34] R. J. Liotta, E. Maglione, N. Sandulescu, T. Vertse, Phys. Lett. B **367**, 1 (1996).
- [35] N. Michel, W. Nazarewicz, M. Ploszajczak, and K. Bennaceur, Phys. Rev. Lett. **89**, 042502 (2002).
- [36] P. Horodecki, Phys. Rev. A **62**, 052716 (2000).
- [37] M. G. Fuda, Phys. Rev. C **64**, 027001 (2001).
- [38] S. S. Zhang, J. Meng, S. G. Zhou, and G. C. Hillhouse, Phys. Rev. C **70**, 034308 (2004).
- [39] L. Zhang, S. G. Zhou, J. Meng, and E. G. Zhao, Phys. Rev. C **77**, 014312 (2008).
- [40] J. Grineviciute and D. Halderson, Phys. Rev. C **85**, 054617 (2012).
- [41] B. N. Lu, E. G. Zhao, and S. G. Zhou, Phys. Rev. Lett. **109**, 072501 (2012); *ibid*, Phys. Rev. C **88**, 024323 (2013).
- [42] T. T. Sun, S. Q. Zhang, Y. Zhang, J. N. Hu, and J. Meng, Phys. Rev. C **90**, 054321 (2014).
- [43] N. Li, M. Shi, J. Y. Guo, Z. M. Niu, and H. Z. Liang, Phys. Rev. Lett. **117**, 062502 (2016).
- [44] B. Serot and J. D. Walecka, Adv. Nucl. Phys. **16**, 1 (1986).
- [45] P. Ring, Prog. Part. Nucl. Phys. **37**, 193 (1996).
- [46] D. Vretenar, A. V. Afanasjev, G. A. Lalazissis, and P. Ring, Phys. Rep. **409**, 101 (2005).
- [47] J. Meng, H. Toki, S. G. Zhou, S. Q. Zhang, W. H. Long, and L. S. Geng, Prog. Part. Nucl. Phys. **57**, 470 (2006).
- [48] T. Nikšić, D. Vretenar, P. Ring, Prog. Part. Nucl. Phys. **66**, 519 (2011).
- [49] H. Z. Liang, J. Meng, and S. G. Zhou, Phys. Rep. **570**, 1 (2015).
- [50] J. Meng and S. G. Zhou, J. Phys. G **42**, 093101 (2015).
- [51] B. Sun, F. Montes, L. S. Geng, H. Geissel, Yu. A. Litvinov, and J. Meng, Phys. Rev. C **78**, 025806 (2008).
- [52] Z. M. Niu, B. Sun, and J. Meng, Phys. Rev. C **80**, 065806 (2009).
- [53] X. D. Xu, B. Sun, Z. M. Niu, Z. Li, Y.-Z. Qian, and J. Meng, Phys. Rev. C **87**, 015805 (2013).
- [54] Z. M. Niu, Y. F. Niu, H. Z. Liang, W. H. Long, T. Nikšić, D. Vretenar, and J. Meng, Phys. Lett. B **723**, 172 (2013).
- [55] Z. M. Niu, Y. F. Niu, Q. Liu, H. Z. Liang, and J. Y. Guo, Phys. Rev. C **87**, 051303(R) (2013).
- [56] Z. P. Li, J. Meng, Y. Zhang, S. G. Zhou, and L. N. Savushkin, Phys. Rev. C **81**, 034311 (2010).
- [57] X. D. Xu, S. S. Zhang, A. J. Signoracci, M. S. Smith, and Z. P. Li, Phys. Rev. C **92**, 024324 (2015).